Original paper

Hydrogen decrepitation of high-entropy rare-earth alloys: Structure and magnetic properties of the formed trihydrides

P.A. Krot, Yu.A. Ovchenkova, N.Yu. Pankratov, I.S. Tereshina, V.N. Verbetsky
Lomonosov Moscow State University, Moscow, Russia
pavelakrot@gmail.com

DOI: 10.26456/pcascnn/2026.18.687

Abstract: The synthesis and investigation of the structural and magnetic properties of the trihydrides of high entropy rare-earth alloys was carried out. It was determined that the alloys containing only heavy rare-earth elements adopted the magnesium-type structure (space group $P6_3/mmc$), while the one made of both heavy and light rare-earth elements had the rhombohedral lattice of samarium type ($R\bar{3}m$). For all the studied trihydrides the complex hexagonal holmium trihydride-type structure ($P\bar{3}c1$) was found. Hydrogen uptake in the alloys led to the lattice expansion, the occurrence of stress and spontaneous cracking along the grain boundaries, as a result of which the ingot crumbled into powder without mechanical grinding. Lanthanide contraction effect for both the studied alloys and their trihydrides was observed. The paramagnetic Curie temperatures, effective magnetic moments, and the prevailing type of exchange interaction were determined for each trihydride. It was found out that hydrogen uptake suppressed magnetic ordering down to 2 K.

Keywords: high-entropy alloys, rare-earths, hydrides, magnetic properties, crystal structure, lanthanide contraction.

Pavel A. Krot – 4th year postgraduate student, Department of Chemistry, Lomonosov Moscow State University
Yulia A. Ovchenkova – Ph. D., Associate Professor, Department of Physics, Lomonosov Moscow State University, ORCID: 0000-0002-2278-9191
Nikolay Yu. Pankratov – Ph. D., Senior Lecturer, Department of Physics, Lomonosov Moscow State University, ORCID: 0000-0003-1565-2661
Irina S. Tereshina – Dr. Sc., Leading Researcher, Department of Physics, Lomonosov Moscow State University, ORCID: 0000-0003-3633-3440
Viktor N. Verbetsky – Dr. Sc., Professor, Department of Chemistry, Lomonosov Moscow State University

УДК 537.622 *Оригинальная статья*

Водородное охрупчивание высокоэнтропийных сплавов редкоземельных элементов: структура и магнитные свойства образующихся тригидридов

П.А. Крот, Ю.А. Овченкова, Н.Ю. Панкратов, И.С. Терёшина, В.Н. Вербецкий
ФГБОУ ВО «Московский государственный университет имени М.В. Ломоносова»
119991, Россия, Москва, ул. Ленинские горы, 1, стр. 3 (ГСП-1)

DOI: 10.26456/pcascnn/2026.18.687

Аннотация: Проведены синтез и исследование структурных и магнитных свойств тригидридов высокоэнтропийных редкоземельных сплавов. Определено, что сплавы, содержащие только тяжелые редкоземельные элементы, имели структуру типа магния (пространственная группа $P6_3/mmc$), тогда как сплав, содержащий как тяжелые, так и легкие редкоземельные элементы, кристаллизовался в ромбоэдрической решетке типа самария ($R\bar{3}m$). Для всех изученных тригидридов установлена сложная гексагональная структура типа тригидрида гольмия ($P\bar{3}c1$). Введение водорода в сплавы привело к расширению их решеток, возникновению напряжений и самопроизвольному растрескиванию по границам зерен, в результате которого слиток рассыпается в порошок без механического помола. Для рассмотренных сплавов, а также для их тригидридов, отмечено явление лантаноидного сжатия. Для каждого из тригидридов определены парамагнитная точка Кюри, эффективный магнитный момент и преобладающий характер обменных взаимодействий. Найдено, что введение водорода подавляет магнитное упорядочение выше 2 К.

© P.A. Krot, Yu.A. Ovchenkova, N.Yu. Pankratov, I.S. Tereshina, V.N. Verbetsky, 2026

Ключевые слова: высокоэнтропийные сплавы, редкие земли, гидриды, магнитные свойства, кристаллическая структура, лантаноидное сжатие.

Крот Павел Андреевич – аспирант 4-го года обучения химического факультета ФГБОУ ВО «Московский государственный университет имени М.В. Ломоносова»
Овченкова Юлия Амирановна – к.ф.-м.н., доцент физического факультета ФГБОУ ВО «Московский государственный университет имени М.В. Ломоносова»
Панкратов Николай Юрьевич – к.ф.-м.н., старший преподаватель физического факультета ФГБОУ ВО «Московский государственный университет имени М.В. Ломоносова»
Терёшина Ирина Семеновна – д.ф.-м.н., ведущий научный сотрудник физического факультета ФГБОУ ВО «Московский государственный университет имени М.В. Ломоносова»
Вербецкий Виктор Николаевич – д.х.н., профессор химического факультета ФГБОУ ВО «Московский государственный университет имени М.В. Ломоносова»

Поступила в редакцию/received: 20.07.2026; после рецензирования/revised: 22.08.2026; принята/accepted 26.08.2026.

1. Introduction

High-entropy alloys (HEAs), composed of five or more elements in equiatomic or near-equiatomic proportions, represent one of the most rapidly developing classes of modern materials [1-4]. Thanks to unique synergistic effects – such as severe lattice distortion and sluggish diffusion – HEAs exhibit physicochemical properties unattainable in traditional alloys [5-8]. High-entropy alloys based on rare earth elements (REE) are of particular interest. The high affinity of REEs for hydrogen offers broad prospects for using such systems, for example, as effective, high-capacity materials for solid-state hydrogen storage [9-13]. The hydrogenation process of HEAs is accompanied by a radical change in their mechanical behavior. The incorporation of hydrogen into the interstitial sites of the highly distorted crystal lattice leads to significant increase in internal stresses, the complete blocking of dislocation glide, and, consequently, extreme embrittlement of the material [14-18]. The described mechanism (hydrogen embrittlement) is the classical physicochemical basis of the HD and HDDR (Hydrogenation-Dehydrogenation-Disproportionation-Recombination) method, which is actively used to obtain nanostructured high-coercivity $Nd-Fe-B$ magnets [19-21].

On the one hand, this phenomenon limits the structural application of the alloys, but on the other, it creates a unique technological opportunity for their subsequent mechanical comminution. Brittle, coarse-grained rare-earth element/heavy rare-earth element-based (REE-HREE) hydrides can be easily converted into a nanocrystalline state via high-energy ball milling without any risk of plastic deformation or material adhesion to the grinding media [22-24].

It is well known that the transition from coarse-grained structures to nanosized powders radically alters the functional properties of systems, including hydrides [25-28]. Reducing particle size to the nanoscale leads to changes in the density of electronic states and reorganization of the magnetic domain structure. At the same time, surface effects begin to play a dominant role [29-32]. In the case of REE hydrides – whose magnetic properties are governed by complex long-

range exchange mediated by conduction electrons (RKKY interaction) and the local magnetic anisotropy of REE ions – the size factor (powder particle size) is expected to exert a decisive influence on magnetic ordering, coercivity, and the Curie or Néel temperature [33-36].

However, a correct identification and interpretation of size effects in nanostructured hydrides require a detailed understanding of the physics of the initial state. Without knowledge of fundamental characteristics of fine-dispersed powders (the grain size is between 1,0 and 10 μm without additional grinding), it is impossible to distinguish between the effects of particle size and those of structural defects, including those introduced during milling.

This paper presents a systematic study of the magnetic properties of rare-earth HEA hydrides in the initial (pre-milling) state. The obtained results provide a reference for further investigations of magnetic phase transitions during controlled nanocrystallization of these systems.

2. Materials and Methods

Seven equiatomic rare-earth alloys were synthesized by arc-melting over a water-cooled copper hearth under an argon atmosphere. Iodide-process titanium was used as a getter. Every alloy was re-melted three times for better chemical homogeneity. Each metal used in arc-melting was of 99,9 wt.% purity or higher. The seven alloy compositions are listed in Table 1 below. The formulas of hydrides are given with the coefficients of REEs equal to one but retaining the hydrogen/metal ratio. Stoichiometry of the alloys was estimated with the help of an energy dispersive spectrometer (EDS) in a scanning electron microscopy (SEM) with field emission using a LEO EVO 50 XVP (Carl Zeiss) microscope operated at 20 kV. The alloys were subjected to annealing in a quartz tube under vacuum (~10^{-3} Pa) for 240 hours. The annealing temperature was set to be ~70% of the lowest calculated melting point of the alloys in a tube:

$$T_{alloy} = \sum_i X_i T_i , \quad (1)$$

where T_{alloy} is the calculated melting point of the alloy, X_i is the atomic fraction of the i-th element, T_i is the melting point of the i-th element.

The synthesized alloys were hydrogenated in a custom-built Sieverts apparatus in order to produce the trihydride compositions, i.e. the ones with the hydrogen/metal ratio H/M between 2,95 to 3,00. To investigate the possible spontaneous decrepitation, each composition was subjected to multiple cycles of hydrogenation-dehydrogenation, with each cycle conducted over a 24 hours timespan. Initial hydrogenation required an elevated temperature of about 200-300°C in each case with subsequent absorptions taking place at room-temperatures, while dehydrogenations were carried out at 900-1000°C. The absorption was considered complete if the hydrogen pressure remained

unchanged for at least 30 min. Van der Waals equation was used to calculate the amount of hydrogen absorbed (and hence the stoichiometry of the hydrides) according to the pressure drop in the system.

The phase composition and structures of the as-cast alloys (hereinafter simply referred to as the «alloys») and their hydrides were evaluated by means of XRD-analysis on a ARL X'TRA (Thermo Fisher Scientific) diffractometer with CuKα radiation. The Rietveld refining was applied to the diffraction patterns with the help of RIETAN-2000 software. Diffraction patterns were produced from powdered hydrides, whereas metallographic specimens of the alloys were used for alloy XRD-analysis.

The magnetization of the trihydrides was measured using a pendulum magnetometer in fields up to 1 T in the 80-300 K temperature range. Moreover, for one of the samples, namely ($GdTbDyErH_{12}$), magnetization was also measured using a SQUID magnetometer in fields up to 1 T in the lower temperature range, namely from 2 to 80 K.

3. Results and Discussion

Analysis of X-ray data revealed that all but one of the alloys crystallized in the HCP lattice of the magnesium structure type, space group $P6_3/mmc$. This is consistent with the ability of heavy rare earth elements to form solid solutions with one another: individual heavy rare earth elements crystallize in the magnesium structure type. For each of the hydrogenated alloys an H/M ratio of 2,95 to 3,00 by applying the van der Waals equation to the pressures registered in the Sieverts apparatus before and after the hydrogenation process, i.e. the studied hydrogenated alloys were trihydrides. Every trihydride crystallized in the complex hexagonal lattice, space group $P\bar{3}c1$, forming a lattice of the holmium trihydride HoH_3 type. This is again consistent with the fact that the trihydrides of individual heavy rare earths crystallize in the HoH_3 structure type. X-ray diffraction patterns of the $YGdTbDy$ alloy and the respective trihydride are shown in Fig. 1 a and 1 b, respectively. The only exception among the alloys is the one containing both HREEs and LREEs, namely $YPrNdTbDy$: it crystallizes in the rhombohedral 9R-samarium-type structure, space group $R\bar{3}m$. The unit cell corresponding to this lattice is hexagonal, enlarged several times along the c-axis. Samarium type-structures were reported for binary alloys composed of an LREE and an HREE in comparable proportions [37-38]. As was already mentioned, the trihydride $Y\,\mathrm{Pr}\,NdTbDyH_{15}$ was found to have the HoH_3 structure, like the other six studied hydrides. This observation is in agreement with the published structures, as samarium trihydride SmH_3 has the same HoH_3 structure as the other HREEs [39, 40]. In every X-ray pattern for both the alloys and their trihydrides several lines not characteristic of the aforementioned structures were observed. The lines

correspond to an FCC structure and are attributed, based on literature, to rare-earth oxides R_2O_3 (R corresponds to all REEs in the alloy) formed at grain boundaries of the alloys and their hydrides [41, 42]. Li et al. and Soler et al. specify that this secondary phase is Y_2O_3 for yttrium-containing REE alloys, which is known to be non-magnetic [18, 43]. Rietveld analysis revealed that this admixture phase constituted between 1,0 and 2,0 vol.% of every studied system. EDS analysis revealed the presence of an oxygen-rich admixture phase in each of the alloys, while also confirming the near-equiatomic ratios of REEs in the synthesized alloys.

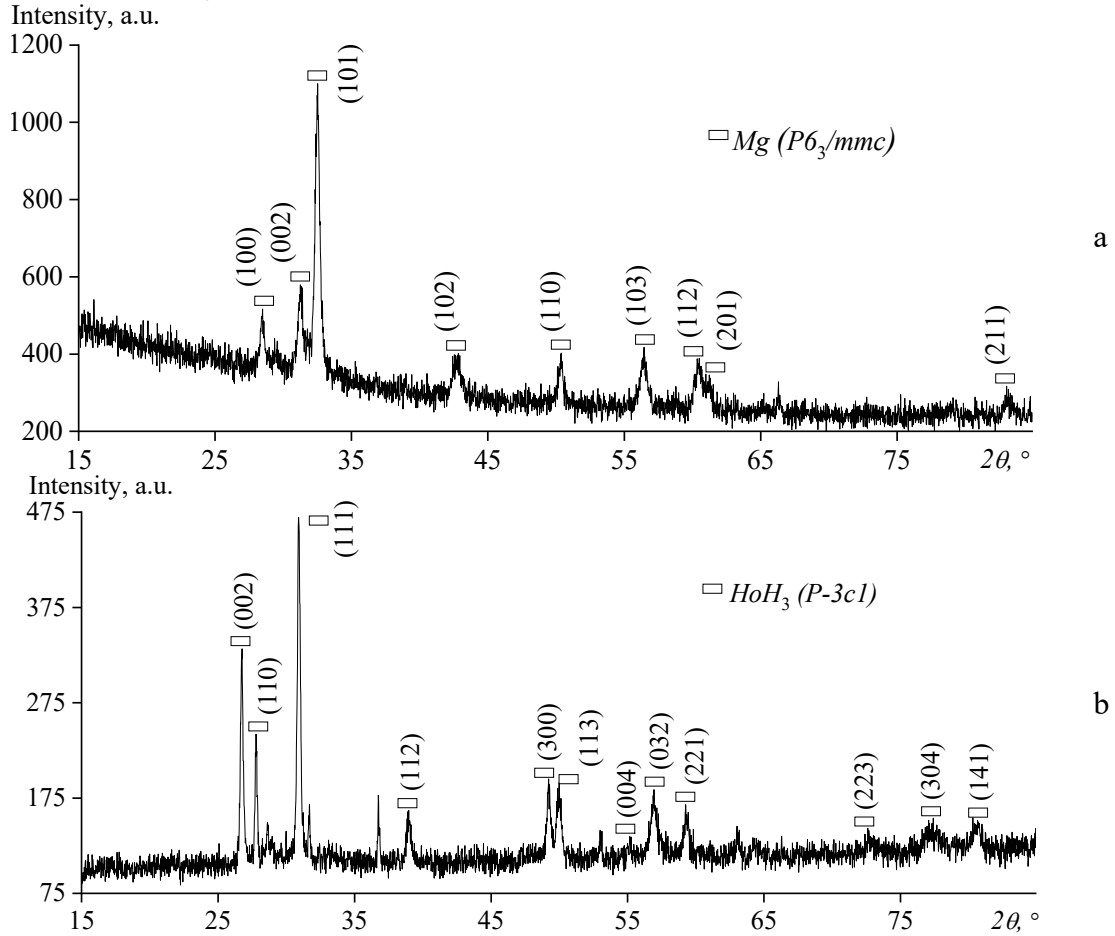

Fig. 1. X-ray patterns of the a) $YGdTbDy$ alloy and b) its trihydride $YGdTbDyH_{12}$.

Notably, the investigated alloys, which exhibited high resistance to manual milling in the as-cast state, turned brittle and could readily be ground to fine powder in a mortar. Moreover, when subjected to multiple (three to four) cycles of hydrogenation-dehydrogenation, each studied alloy transformed into fine powder, which can facilitate their subsequent transformation into nanopowder by means of mechanical milling.

Tables 1 a and 1 b give the lattice parameters, unit cell volumes per formula unit V/Z (HCP is the hexagonal close-packed, Hex. is the complex hexagonal structure: REEs form an HCP-structure, hydrogen occupies interstitial sites).

Table 1 a. Structures and calculated lattice parameters of the studied alloys and their respective trihydrides.

Alloy / trihydride	Structure	$a=b$, Å	c, Å	c/a
YGdTbDy	HCP, Mg, $P6_3/mmc$	3,62(2)	5,72(1)	1,58
YGdTbDyHo	HCP, Mg, $P6_3/mmc$	3,61(3)	5,68(9)	1,57
YGdTbDyEr	HCP, Mg, $P6_3/mmc$	3,61(4)	5,67(3)	1,57
GdTbDyEr	HCP, Mg, $P6_3/mmc$	3,60(3)	5,66(0)	1,57
YTbDyEr	HCP, Mg, $P6_3/mmc$	3,59(1)	5,70(2)	1,59
YGdDyEr	HCP, Mg, $P6_3/mmc$	3,59(2)	5,69(4)	1,59
YTbDyPrNd	9R, Sm, $R\bar{3}m$	3,62(0)	26,03(8)	7,19
$YGdTbDyH_{12}$	Hex., HoH_3, $P\bar{3}c1$	6,41(3)	6,66(4)	1,04
$YGdTbDyHoH_{15}$	Hex., HoH_3, $P\bar{3}c1$	6,36(2)	6,58(7)	1,04
$YGdTbDyErH_{15}$	Hex., HoH_3, $P\bar{3}c1$	6,38(4)	6,63(0)	1,04
$GdTbDyErH_{12}$	Hex., HoH_3, $P\bar{3}c1$	6,37(1)	6,61(9)	1,04
$YTbDyErH_{12}$	Hex., HoH_3, $P\bar{3}c1$	6,34(4)	6,59(0)	1,04
$YGdDyErH_{12}$	Hex., HoH_3, $P\bar{3}c1$	6,36(8)	6,62(7)	1,04
$YTbDyPrNdH_{15}$	Hex., HoH_3, $P\bar{3}c1$	6,47(9)	6,70(9)	1,04

Table 1 b. Unit cell volumes per formula unit, densities, both calculated according to X-ray patterns and the rule of mixtures, of the alloys and trihydrides.

Alloy / trihydride	V/Z, Å^3	$\rho(X)$, g/cm^3	$\rho(mix)$, g/cm^3
YGdTbDy	32,45	7,26	7,29
YGdTbDyHo	32,11	7,58	7,59
YGdTbDyHo	32,00	7,63	7,64
GdTbDyEr	31,75	8,45	8,44
YTbDyEr	31,81	7,54	7,58
YGdDyEr	31,75	7,53	7,50
YTbDyPrNd	32,84	7,04	7,01
$YGdTbDyH_{12}$	39,50	6,09	6,13
$YGdTbDyHoH_{15}$	38,77	6,41	6,38
$YGdTbDyErH_{15}$	38,95	6,40	6,43
$GdTbDyErH_{12}$	38,77	7,05	7,04
$YTbDyErH_{12}$	38,23	6,41	6,39
$YGdDyErH_{12}$	38,83	6,29	6,33
$YTbDyPrNdH_{15}$	40,67	5,81	5,85

Note: $\rho(X)$ – density calculated from X-ray data, $\rho(mix)$ – density calculated by the rule of mixtures.

Finally, they compare the calculated X-ray densities $\rho(X)$ of the studied trihydrides and alloys with the rule of mixtures densities, $\rho(mix)$, i.e., assuming

that the density of the solid solution is equal to the average density of its components, since all the studied alloys are equiatomic:

$$\rho(mix) = \sum_i X_i \rho_i \,, \tag{2}$$

where X_i is the atomic fraction of the i-th element, ρ_i is the density of the i-th component. For the alloy trihydrides, their calculated densities were estimated as the weighted averages of the densities of the trihydrides of the constituent REEs. The H/M in each composition was ~3,0. Calculated density estimate is in good agreement with the X-ray density, confirming the formation of solid solutions with minimal influence of impurity phases. In each case, two obtained density values for the same alloy/trihydride differ by no more than 1%. The greatest deviation from the rule of mixtures is in the case of $YTbDyPrNdH_{15}$: its X-ray density stands at 99,3% of the density, calculated according to the rule of mixtures.

The unit cell volumes per formula unit V/Z of the hydrides are larger than those of the corresponding alloys. Upon hydrogenation, the V/Z value increased by about 22% on average for all alloys, with individual values ranging from 20,2% for $YGdTbDy$ to 23,8% for $YPrNdTbDy$. This is consistent with the literature data on the hydrides of both individual light and heavy rare earths: the introduction of hydrogen leads to considerable lattice expansion [11, 39].

It is also possible to track changes in lattice parameters and volumes as a function of alloy composition. The phenomenon of lanthanide contraction, i.e. a monotonic decrease in the atomic and ionic radii of rare-earth elements when going from lighter to heavier ones, is well known [44]. One can assign an effective atomic number $\bar{N}$ to REE alloys and their trihydrides calculated as

$$\bar{N} = \sum_i X_i N_i \,, \tag{3}$$

where X_i is the atomic fraction of the i-th element, N_i is the its atomic number. In the yttrium case, which is not a member of the lanthanide group, it was assigned an effective atomic number based on its metallic radius and the empirical dependence of the radius on the atomic number for lanthanides. If we plot the unit cell volume of the resulting alloys as a function of their N_i, we can observe a phenomenon analogous to lanthanide contraction: the unit cells get more compressed as the $\bar{N}$ increases (see Fig. 2). When a heavier REE substitutes a lighter REE it leads to a unit cell compression. In the case of the trihydrides, contraction occurs more rapidly as the effective atomic number increases.

Magnetization measurements at temperatures from 80 to 300 K revealed paramagnetic behavior for all studied trihydrides across the entire temperature range. The inverse susceptibility dependence on temperature is linear and follows the Curie-Weiss law:

$$\chi = C/(T - \theta_p) \,, \tag{4}$$

where χ is the magnetic susceptibility, $cm^3 \cdot mol^{-1}$, C is the Curie constant, θ_p is the paramagnetic Curie temperature, and T is temperature.

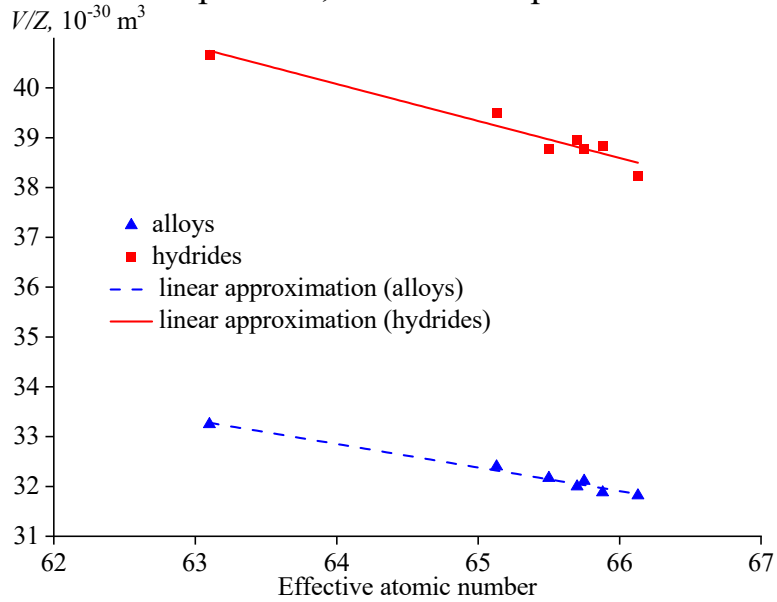

Fig. 2. Unit cell volume per formula unit vs. the effective atomic number of the investigated alloys and their respective trihydrides.

As an example, the magnetization of $YGdTbDyH_{12}$ trihydride is shown in Fig. 3 as a function of the field for different temperatures. It is evident that the spontaneous magnetic moment here is absent. The magnetic susceptibility of the hydrides at a given temperature was calculated from the slopes of the linear curves, then the parameters C and θ_p were calculated according to (4). The effective magnetic moments μ_{eff} of the investigated samples, expressed in units of μ_B, were calculated according to the following formula:

$$\mu_{eff} = \sqrt{\frac{3k_B C}{N_A \mu_B}}, \tag{5}$$

where k_B is the Boltzmann constant, C is the molar Curie constant, calculated using previously measured magnetization curves and XRD densities of the hydrides, N_A is the Avogadro constant, μ_B is the Bohr magneton [45]. The paramagnetic Curie temperatures and the effective magnetic moments, as well as the de Gennes factors of the alloys $\bar{G}$ and the theoretic magnetic moments $\mu_{eff}(theoretical)$ are presented in Table 2. The theoretical magnetic moments were calculated assuming that the de Gennes factors of rare-earth alloys and their hydrides are linear combinations of the de Gennes factors of their constituent metals:

$$\bar{G} = \sum_i X_i G_i, \tag{6}$$

$$\mu_{eff}(theoretical) = \sum_i X_i \mu_i, \tag{7}$$

where X_i, μ_i and G_i are the mole fraction (for hydrides, the mole fraction among REEs were taken), the theoretical magnetic moment, and de Gennes factor of the i-th REE in a given alloy or hydride, respectively [46]. De Gennes factors of individual REEs can be found in published works [47].

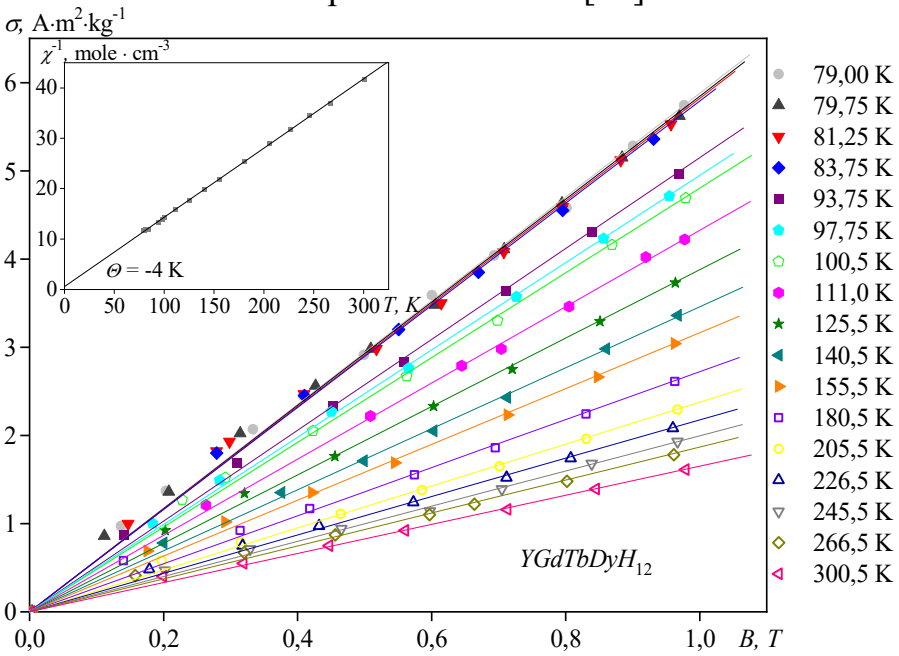

Fig. 3. Magnetization curves at various temperatures for $YGdTbDyH_{12}$ trihydride. Insert: the calculated inverse susceptibility as a function of temperature.

From the available works it is known that the HREE alloys possess Néel temperatures falling in the 100 to 200 K temperature range [41, 48-50]. After the alloys were hydrogenated until the H/M ratio was near 3,0, no magnetic ordering was observed above 80 K for any of the investigated compositions. For each trihydride the paramagnetic temperatures were calculated to be slightly below or above 0 K, with former indicating a weak negative interaction between the metallic ions (anti-ferromagnetism) and the latter suggesting a weak positive interaction (ferromagnetism). The effective magnetic moment of every trihydride is close to the respective theoretically calculated moment and exceeds it by no more than 15%. Such an excessive magnetic moment compared to the theoretically magnetic moments for rare-earth alloys, especially for the yttrium containing alloys, was reported in [51] and is explained by the polarization of the conducting band of the electronic system of a given alloy. The $GdTbDyErH_{12}$ composition, having the biggest de Gennes factor and the absolute value of the paramagnetic Curie temperature among the investigated trihydrides, was subjected to additional magnetization measurements at low temperatures. Magnetization of the $GdTbDyErH_{12}$ trihydride was measured in the 2 to 50 K temperature range and in fields up to 1 T. The temperature dependence of magnetic moment measured in a weak magnetic field (0,1 T) is shown in Fig. 4. No inflection points were found on the magnetization curve measured at 0,1 T.

Table 2. Curie-Weiss magnetic parameters of the obtained trihydrides and their weighted de Gennes factors.

Trihydride	θ_p, K	μ_{eff}, μ_B	$\bar{G}$	$\mu_{eff}(theoretical)$, μ_B
$YGdTbDyH_{12}$	-4,0	7,20	8,33	7,08
$YGdTbDyHoH_{15}$	0,8	8,82	7,57	7,78
$YGdTbDyErH_{15}$	-8,8	7,92	7,18	7,58
$GdTbDyErH_{12}$	-12,9	9,99	8,97	9,48
$YTbDyErH_{12}$	1,3	7,99	5,03	7,49
$YGdDyErH_{12}$	-0,4	8,16	6,35	7,05
$YTbDyPrNdH_{15}$	2,8	6,35	3,90	5,51

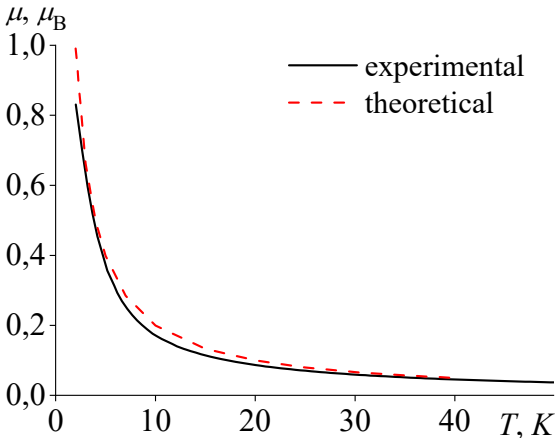

Fig. 4. Magnetic moment vs. temperature plot for $GdTbDyErH_{12}$ trihydride, $\mu_0 H = 0{,}1$ T. The theoretical dependence was calculated for an ideal paramagnet.

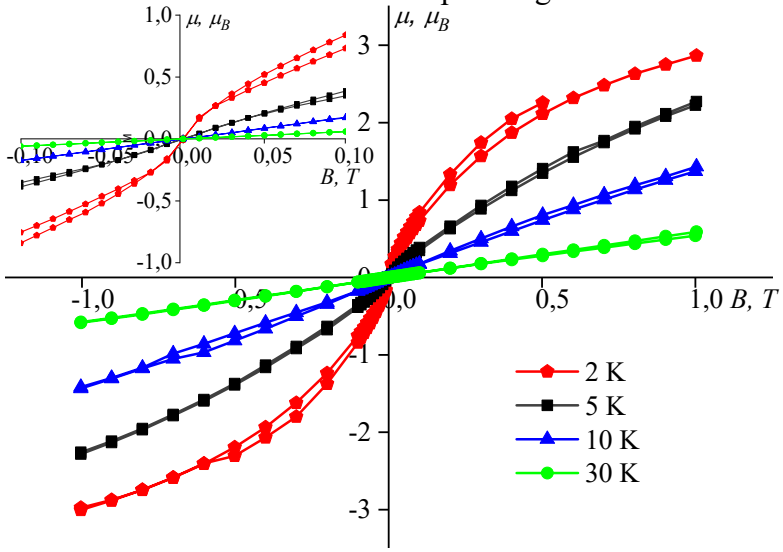

Fig. 5. Magnetization curves for $GdTbDyErH_{12}$ trihydride for various temperatures from 2 to 30 K. Insert: close-up view of the curves at the center.

Magnetization curves for $GdTbDyErH_{12}$ trihydride are plotted in Fig. 5. No spontaneous magnetization is observed on any of the curves, however for

temperatures below 10 K and in magnetic fields higher than a certain critical value (0,02 T for 2 K and 0,06 T for 5 K) the curves have a slight hysteresis.

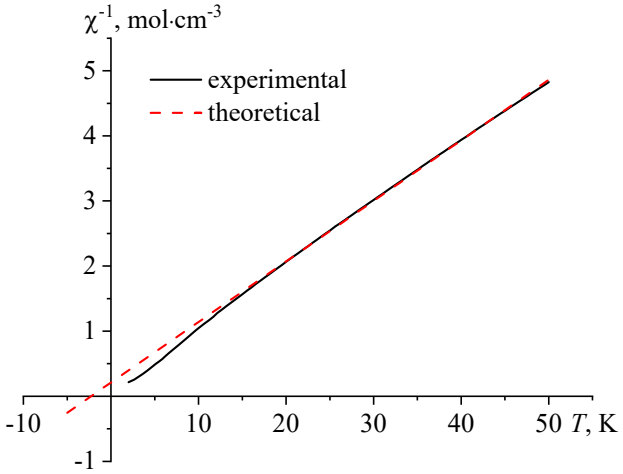

Fig. 6. Inverse susceptibility vs. temperature for $GdTbDyErH_{12}$ trihydride.

The temperature dependence of the inverse susceptibility above 15 K is linear and is in good agreement with the Curie-Weiss law (see Fig. 6). The experimental curve deviates noticeably from the calculated curve below 15 K. The values of the effective magnetic moment and paramagnetic Curie point equal to 9,4 μ_B and -2,4 K, respectively. The calculated inverse magnetic susceptibility curve intersects the temperature axis in the negative region, indicating the predominance of antiferromagnetic ordering in this trihydride. One can see that the magnetization curves at low temperatures are nonlinear, but no peculiarities are observed in the temperature dependence of magnetization. However, it is known that at low temperatures, when the magnetic field energy becomes comparable to kT, even for an ideal paramagnet, the dependence of magnetization on the field becomes nonlinear. To verify this, knowing the magnetic moment values, the magnetization dependences on temperature and magnetic field under the assumption that the sample is an ideal paramagnet were calculated. The calculations were compared with experimental data. In accordance with [47], the obtained data were analyzed by calculating the theoretical dependences of the magnetic moment on temperature and magnetic field for an ideal paramagnet using the following formulas:

$$\langle \mu_Z \rangle = g_J \mu_B J B_J(x), \tag{8}$$

$$B_J(x) = \frac{2J+1}{2J} coth(\frac{2J+1}{2J} x) - \frac{1}{2J} coth(\frac{x}{2J}), \tag{9}$$

$$x = g_J \mu_B JB / k_B T, \tag{10}$$

where g_J is the Landé g-factor, J is the total angular momentum quantum number, B is the external magnetic field. The g and J values for alloys were calculated in two different ways. First, the mean values of g and J of the ions of REEs constituting the alloys were used. Second, the $\mu(T,B)$ relationships for

individual rare-earth metals were calculated and added together, bearing in mind that the alloys in question are equiatomic. Both methods yield results that are in good agreement with each other.

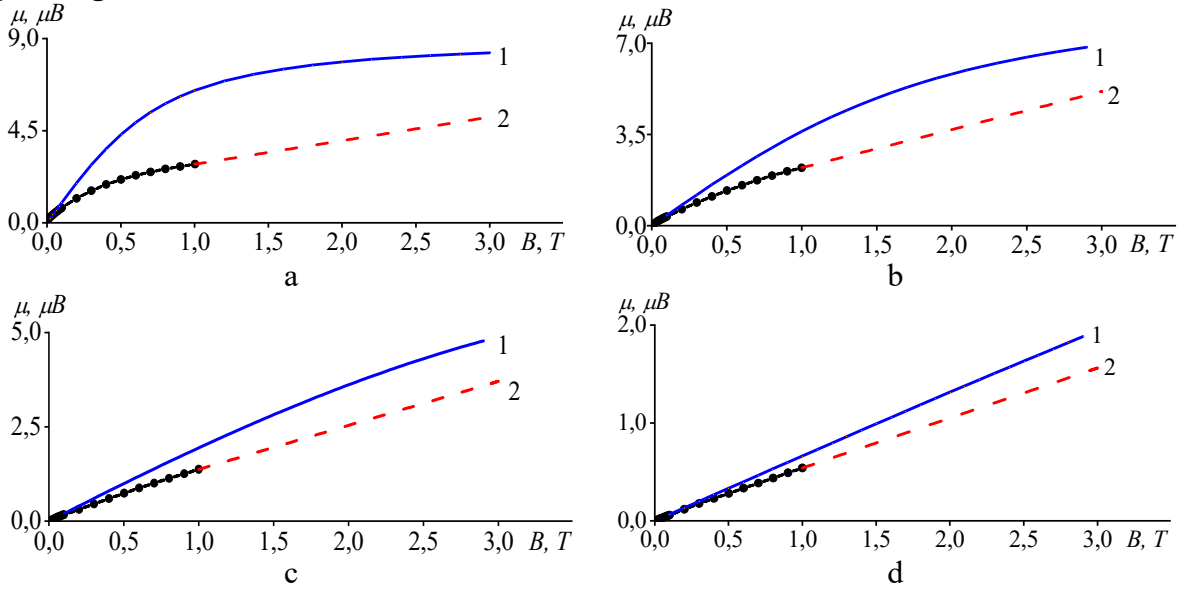

Fig. 7. Magnetic moment vs. magnetic field for $GdTbDyErH_{12}$ trihydride at (a) 2K, (b) 5 K, (c) 10 K and (d) 30 K. Solid lines (1) correspond to the ideal paramagnet model, symbols (2) represent experimental data, and the dashed line shows the calculated extrapolation.

The calculated temperature dependence of the magnetic moment of an ideal paramagnet for a weak magnetic field of 0,1 T is close to the dependence established experimentally (see Fig. 4). This means that in a weak magnetic field, the behavior of the trihydride is similar to that of an ideal paramagnet. As the temperature rises, magnetization of the $GdTbDyErH_{12}$ continuously decreases with no inflection points on the curve.

However, in higher magnetic fields, the observed values of magnetic moment diverge significantly from the ones calculated assuming that the investigated trihydride behaves as an ideal paramagnet. Fig. 7 shows the corresponding experimental curves and the calculated dependences assuming that the trihydride is an ideal paramagnet. At 2 K, the experimentally measured magnetization in a field of 1 T is almost half the theoretical value, which should be observed in an ideal paramagnet. As the temperature increases, the differences become smaller, and at 30 K, there is no significant divergence between the calculated and experimental values in fields less than 0,5 T.

Thus, measurements at low temperatures revealed a decrease in magnetization in a magnetic field compared to the model of non-interacting spins. To explain this effect, two factors should be considered. Firstly, it is known that the initial majority-HREE rare-earth alloys are characterized by non-collinear ordering [51, 52], i.e., there is a competition of positive and negative exchange interactions between moments located in different crystallographic positions. The

negative paramagnetic point in $GdTbDyErH_{12}$ trihydride also indicates the presence of a weak and negative exchange interaction between magnetic moments, which may lead to a decrease in magnetization in an external field. Moreover, it has been reported that the trihydrides of individual heavy rare-earths, such as GdH_3, DyH_3 and ErH_3, order antiferromagnetically at 1,8 K, 3,2 K, and 0,6 K, respectively [53-55]. Secondly, the rare-earth ions constituting the alloys in question are known to have high magnetocrystalline anisotropy, which can hinder the orientation of magnetic moments along the field, also potentially reducing the resulting magnetic moment.

5. Conclusions

On the one hand, all the trihydrides of rare-earth high-entropy alloys synthesized for the first time in this work crystallized in the complex hexagonal holmium trihydride-type structure (space group $P\bar{3}c1$), regardless of the type and stoichiometry of the rare earths constituting them. On the other hand, the crystal structures of the respective alloys were found to be dependent on their composition: the alloys made of only heavy rare earths adopted the HCP magnesium-type structure ($P6_3/mmc$), while the alloy containing 40 and 60 at.% of light and heavy rare-earths respectively had the rhombohedral samarium-type structure ($R\bar{3}m$). The lanthanide contraction effect was observed for both the synthesized alloys and their trihydrides.

Introduction of hydrogen into the crystal lattices of the investigated rare-earth high-entropy alloys led to their expansion (~20% in each case) and generated considerable strain. This gave rise to the spontaneous decrepitation: after three to four cycles of hydrogenation-dehydrogenation, the massive as-cast ingots of the alloys transformed into fine powder. This can facilitate the production of nanosized materials out of these alloys by means of mechanical milling.

Based on the temperature and field dependences of the magnetization for each investigated trihydride, their key magnetic characteristics were calculated: paramagnetic Curie temperatures, effective magnetic moments and the prevailing types (signs) of exchange interactions.

It was found that the transformation of the alloys into the respective trihydrides did not significantly change the effective magnetic moments of the rare-earth ions constituting them. However, the change in the crystal structure and the electronic subsystem caused by the introduction of hydrogen suppressed magnetic ordering in each studied trihydride, with the suppression confirmed for temperatures as low as 2 K in the case of $GdTbDyErH_{12}$.

The results of this work provide a basis for subsequent studies of the evolution of magnetic properties in rare-earth HEAs as they undergo a controlled transition to the nanocrystalline state. Study of magnetism of high-entropy rare-

earth systems and their hydrides in a wide temperature range, including room temperature, will allow to assess the prospects of their possible practical applications. Indeed, the cost of such functional materials can be drastically reduced by using readily available mixtures, such as mischmetal, instead of individual rare earths for their production.

The study was carried out as part of the state assignment of Lomonosov Moscow State University (registration number 122012400186-9).

References:

1. Tsai M.-H., Yeh J.-W. High-entropy alloys: a critical review, *Materials Research Letters*, 2014, vol. 2, issue 3, pp. 107-123. DOI: 10.1080/21663831.2014.912690.
2. Miracle D.B., Senkov O.N. A critical review of high entropy alloys and related concepts, *Acta Materialia*, 2017, vol. 122, pp. 448-511. DOI: 10.1016/j.actamat.2016.08.081.
3. Gromov V.E., Konovalov S.V., Ivanov Y.F., Osintsev K.A. Structure and properties of high-entropy alloys, *Advanced Structured Materials*, vol. 107. Cham, Springer, 2021, X+110 p. DOI: 10.1007/978-3-030-78364-8.
4. Yang C. Advances in high-entropy alloys' microstructure, properties and preparation, *Metals*, 2026, vol. 16, issue 6, pp. 607-610. DOI: 10.3390/met16060607.
5. Miracle D.B. High-entropy alloys: a current evaluation of founding ideas and core effects and exploring «nonlinear alloys», *The Journal of the Minerals, Metals and Materials Society*, 2017, vol. 69, issue 11, pp. 2130-2136. DOI: 10.1007/s11837-017-2527-z.
6. Pickering E.J., Jones N.G. High-entropy alloys: a critical assessment of their founding principles and future prospects, *International Materials Reviews*, 2016, vol. 61, issue 3, pp. 183-202. DOI: 10.1080/09506608.2016.1180020.
7. Wang X., Guo W., Fu Y. High-entropy alloys: emerging materials for advanced functional applications, *Journal of Materials Chemistry A*, 2020, vol. 9, issue 2, pp. 663-701. DOI: 10.1039/D0TA09601F.
8. Wang J., Jia D., Gao Q., Fu Y., Wu X. High-entropy alloy coatings: a systematic review on composition design, microstructural mechanisms, and multifunctional application, *Materials & Design*, 2025, vol. 258, art. no. 114715, 5 p. DOI: 10.1016/j.matdes.2025.114715.
9. Mikheeva V.I., Kost M.E. The hydrides of the rare-earth metals, *Russian Chemical Reviews*, 1960, vol. 29, issue 1, pp. 28-37. DOI: 10.1070/RC1960v029n01ABEH001216.
10. Bos W.G., Gayer K.H. The rare earth hydrides, *Journal of Nuclear Materials*, 1966, vol. 18, issue 1, pp. 1-30. DOI: 10.1016/0022-3115(66)90092-4.
11. Korst W.L., Warf J.C. Rare earth-hydrogen systems. I. Structural and thermodynamic properties, *Inorganic Chemistry*, 1966, vol. 5, issue 10, pp. 1719-1726. DOI: 10.1021/ic50044a018.
12. Jiang Z., Wang J. Cao D. Research progress of rare earth-based hydrogen storage alloys, *Key Engineering Materials*, 2020, vol. 861, pp. 354-362. DOI: 10.4028/www.scientific.net/KEM.861.354.
13. Xu Y., Yang X., Li Y. et al. Rare-earth metal-based materials for hydrogen storage: progress, challenges, and future perspectives, *Nanomaterials*, 2024, vol. 14, issue 20, pp. 1671-1690. DOI: 10.3390/nano14201671.
14. Sahlberg M., Karlsson D., Zlotea C. Jansson U. Superior hydrogen storage in high entropy alloys, *Scientific Reports*, 2016, vol. 6, art. no. 36770, 6 p. DOI: 10.1038/srep36770.
15. Karlsson D., Ek G., Cedervall J. et al. Structure and hydrogenation properties of a HfNbTiVZr high-entropy alloy, *Inorganic Chemistry*, 2018, vol. 57, issue 4, pp. 2103-2110. DOI: 10.1021/acs.inorgchem.7b03004.
16. Zlotea C., Sow M.A., Ek G. et al. Hydrogen sorption in TiZrNbHfTa high entropy alloy, *Journal of Alloys and Compounds*, 2019, vol. 775, pp. 667-674. DOI: 10.1016/j.jallcom.2018.10.108.
17. Zhang C., Song A., Yuan Y. et al. Study on the hydrogen storage properties of a TiZrNbTa high entropy alloy, *International Journal of Hydrogen Energy*, 2020, vol. 45, issue 8, pp. 5367-5374. DOI: 10.1016/j.ijhydene.2019.05.214.
18. Li T., Xie Z., Zhou W. et al. Study on the hydrogen absorption properties of a YGdTbDyHo rare-earth high-entropy alloy, *International Journal of Minerals, Metallurgy and Materials*, 2025, vol. 32, issue 1, pp. 127-135. DOI: 10.1007/s12613-024-2933-5.
19. Ragg O.M., Keegan G., Nagel H., Harris I.R. The HD and HDDR processes in the production of Nd-Fe-B permanent magnets, *International Journal of Hydrogen Energy*, 1997, vol. 22, issues 2-3, pp. 333-342. DOI: 10.1016/S0360-3199(96)00174-7.

20. Poenaru I., Patroi E.A., Patroi D., Iorga A., Manta E. HDDR as advanced processing method and recycling technology to address the rare-earth resource criticality in high performance $Nd_2Fe_{14}B$ magnets production, *Journal of Magnetism and Magnetic Materials*, 2023, vol. 577, art. no. 170777, 19 p. DOI: 10.1016/j.jmmm.2023.170777.
21. Liu R., Bulyk I.I., Yang M., Wang Y., Wang H. Features of the solid HDDR process in sintered (Nd,Pr,Gd)-Fe-B magnets at low hydrogen pressure and low temperature, *Materials*, 2025, vol. 18, issue 17, pp. 4019-4036. DOI: 10.3390/ma18174019.
22. Huot J., Cuevas F., Deledda S. et al. Mechanochemistry of metal hydrides: recent advances, *Materials*, 2019, vol. 12, issue 17, art. no. 2778, 44 p. DOI: 10.3390/ma12172778.
23. Duwal S., Stavila V., Spataru C. et al. Enhancement of hydrogen absorption and hypervalent metal hydride formation in lanthanum using cryogenic ball milling, *arXiv:2506.23980*, 2025, 24 p. DOI: 10.48550/arXiv.2506.23980.
24. Pommerin A., Felderhoff M., Schüth F., Weidenthaler C. Influence of the ball milling conditions on the preparation of rare earth aluminum hydrides, *Scripta Materialia*, 2010, vol. 63, issue 11, pp. 1128-1131. DOI: 10.1016/j.scriptamat.2010.08.020.
25. Zaluski L., Zaluska A., Ström-Olsen J.O. Nanocrystalline metal hydrides, *Journal of Alloys and Compounds*, 1997, vols. 253-254, pp. 70-79. DOI: 10.1016/S0925-8388(96)02985-4.
26. Nielsen T.K., Besenbacher F., Jensen T.R. Nanoconfined hydrides for energy storage, *Nanoscale*, 2011, vol. 3, issue 5, pp. 2086-2098. DOI: 10.1039/c0nr00725k
27. Palmero P. Structural ceramic nanocomposites: a review of properties and powders' synthesis methods, *Nanomaterials*, 2015, vol. 5, issue 2, pp. 656-696. DOI: 10.3390/nano5020656.
28. Luo Y., Wang Q., Li J. et al. Enhanced hydrogen storage/sensing of metal hydrides by nano-modification, *Materials Today Nano*, 2019, vol. 9, art. no. 100071, 87 p. DOI: 10.1016/j.mtnano.2019.100071.
29. Preiur D., Bonani W., Popa K. et al. Size dependence of lattice parameter and electronic structure in CeO_2 nanoparticles, *Inorganic Chemistry*, 2020, vol. 59, issue 8, pp. 5760-5767. DOI: 10.1021/acs.inorgchem.0c00506.
30. Jagiello K., Chomicz B., Avromopoulos A. et al. Size-dependent electronic properties of nanomaterials: how this novel class of nanodescriptors supposed to be calculated?, *Structural Chemistry*, 2017, vol. 28., issue 3, pp. 635-643. DOI: 10.1007/s11224-016-0838-2.
31. Caizer C. Nanoparticle size effect on some magnetic properties, *Handbook of Nanoparticles*. Amsterdam, Springer, 2015, pp. 475-519. DOI: 10.1007/978-3-319-15338-4_24.
32. Issa B., Obaidat I.M., Albiss B.A., Yousef H. Magnetic Nanoparticles: Surface Effects and Properties Related to Biomedicine Applications, *International Journal of Molecular Sciences*, 2013, vol. 14, issue 11, pp. 21266-21305. DOI: 10.3390/ijms141121266.
33. Vajda P., Andre G. Commensurate and incommensurate magnetic structures in rare-earth hydrides, *Journal of Alloys and Compounds*, 2001, vol. 326, issues 1-2, pp. 151-156. DOI: 10.1016/S0925-8388(01)01251-8.
34. Piquer C., Grandjean F., Isnard O., Long G.J. A phenomenological model for the rare-earth contribution to the magnetic anisotropy in $RFe_{11}Ti$ and $RFe_{11}TiH$, *Journal of Physics: Condensed Matter*, 2006, vol. 18, no. 1, pp. 221-242, DOI: 10.1088/0953-8984/18/1/016.
35. Skomski R. RKKY interactions between nanomagnets of arbitrary shape, *EDP Sciences Europhysics Letters*, 1999, vol. 48, issue 4, pp. 455-460. DOI: 10.1209/epl/i1999-00504-y.
36. Mi S., Yuan S.-H., Lyu P. Size effect of Ruderman–Kittel–Kasuya–Yosida interaction mediated by electrons in nanoribbons, *Journal of Applied Physics*, 2011, vol. 109, issue 8, art. no. 083931, 4 p. DOI: 10.1063/1.3575338.
37. Lundin C.E. *Research on the samarium-type intermediate phases of intra-rare-earth binary systems*, 633558 (also Given as DRI-2326, Final Report), Denver Research Institute, University of Denver, CO, USA, 1966, 32 p.
38. Jayaraman A., Sherwood R.C., Williams H.J., E. Corenzwit. Pressure-induced phase transformations and magnetic ordering in some intra-rare-earth alloys and samarium, *Physical Review*, 1966, vol. 148, issue 2, pp. 502-508. DOI: https://doi.org/10.1103/PhysRev.148.502.
39. Ellner M., Reule H., Mittemeijet E.J. The structure of the trihydride GdH_3, *Journal of Alloys and Compounds*, 2000, vol. 309, issues 1-2, pp. 127-131. DOI: https://doi.org/10.1016/S0925-8388(00)01055-0.
40. Mansmann M., Wallace W.E. The structure of HoD_3, *Journal de Physique*, 1964, vol. 25, issues 5, pp. 454-459. DOI: 10.1051/jphys:01964002505045400.
41. Uporov S.A., Estemirova S.Kh., Sterkhov E.V. et al. Magnetocaloric effect in ScGdTbDyHo high-entropy alloy: impact of synthesis route, *Intermetallics*, 2022, vol. 151, art. no. 107678, 10 p. DOI: 10.1016/j.intermet.2022.107678.
42. Qiao J.W., Bao M.L., Zhao Y.J. et al. Rare-earth high entropy alloys with hexagonal close-packed structure, *Journal of Applied Physics*, 2018, vol. 124, issue 19, art. no. 195101, 7 p. DOI: 10.1063/1.5051514.
43. Soler R., Evirgen A., Yao M. Microstructural and mechanical characterization of an equiatomic YGdTbDyHo high entropy alloy with hexagonal close-packed structure, *Acta Materialia*, 2018, vol. 156, pp. 86-96. DOI:

10.1016/j.actamat.2018.06.010.
44. Jordan R.B. The lanthanide contraction: what is abnormal and why?, *Inorganic Chemistry*, 2025, vol. 64, issue 5, pp. 2207-2216. DOI: 10.1021/acs.inorgchem.4c03698.
45. Mugiraneza S., Hallas A.M. Tutorial: a beginner's guide to interpreting magnetic susceptibility data with the Curie-Weiss law, *Communications Physics*, 2022, vol. 5, art. no. 95, 12 p. DOI: 10.1038/s42005-022-00853-y.
46. Wang L., Lu H., Guo H. Multi-principal rare-earth Gd-Tb-Dy-Ho-Er alloys with high magnetocaloric performance near room temperature, *Journal of Alloys and Compounds*, 2023, vol. 960, art. no. 170901, 10 p. DOI: 10.1016/j.jallcom.2023.170901.
47. Kudrevatykh N.V., Volegov A.S. *Magnetizm redkhozemelnykh metallov i ikh intermetallicheskikh soedineniy* [Magnetism of rare-earth metals and their intermetallic compounds]. Yekaterinburg, Ural University Publ., 2015, 198 p. (In Russian).
48. Yuan Y., Wu X., Tong X. et al. Rare-earth high-entropy alloys with giant magnetocaloric effect, *Acta Materialia*, 2017, vol. 125, pp. 481-489. DOI: 10.1016/j.actamat.2016.12.021.
49. Lu S.F., Ma L., Rao G.H. et al. Magnetocaloric effect of high-entropy rare-earth alloy GdTbHoErY, *Journal of Materials Science: Materials in Electronics*, 2021, vol. 32, issue 8, pp. 10919-10926. DOI: 10.1007/s10854-021-05749-1.
50. Svalov A.V., Neznakhin D.S., Arkhipov A.V. et al. Magnetocaloric effect in powder of GdTbDyHoEr high-entropy alloy, *Physics of the Solid State*, 2024, vol. 66, issue 12, pp. 2120-2124. DOI: 10.61011/PSS.2024.12.60204.313.
51. Nikitin S.A. *Magnitnye svoystva redkozemelnykh metallov i splavov* [Magnetic properties of rare earth metals and their alloys]. Moscow, Moscow State University Publ., 1989, 248 p. (In Russian).
52. Pankratov N.Yu., Tereshina I.S., Krot P.A., Verbetsky V.N., Nikitin S.A. Structure and magnetic properties of the medium-entropy GdTbDyY alloy, *Bulletin of the Russian Academy of Sciences: Physics*, 2025, vol. 89, issue 4, pp. 572-577. DOI: 10.1134/S1062873825710785.
53. Flood D.J. Crystal fields and magnetic properties of ErH_3, *Journal of Applied Physics*, 1978, vol. 49, issue 3, pp. 1495-1497. DOI: 10.1063/1.324933.
54. Carlin R.L., Chirico R.D., Joung K.O. et al. Magnetic ordering in GdH_3, *Physics Letters A*, 1980, vol. 75, issue 5, pp. 413-414. DOI: 10.1016/0375-9601(80)90858-0.
55. Carlin, R.L., Krause L.J. Magnetic ordering in DyH_2 and DyH_3, *Chemical Physics Letters*, 1981, vol. 82, issue 2, pp. 323-326. DOI: 10.1016/0009-2614(81)85165-2.

Библиографический список:

1. **Tsai, M.-H.** High-entropy alloys: a critical review / M.-H. Tsai, J.-W. Yeh // Materials Research Letters. –2014. – V. 2. – I. 3. – P. 107-123. DOI: 10.1080/21663831.2014.912690.
2. **Miracle, D.B.** A critical review of high entropy alloys and related concepts / D.B. Miracle, O.N. Senkov // Acta Materialia. – 2017. – V. 122. – P. 448-511. DOI: 10.1016/j.actamat.2016.08.081.
3. **Gromov, V.E.** Structure and properties of high-entropy alloys / V.E. Gromov, S.V. Konovalov, Y.F. Ivanov, K.A. Osintsev // In series: Advanced Structured Materials. – V. 107. – Cham: Springer, 2021. – X+110 p. DOI: 10.1007/978-3-030-78364-8.
4. **Yang, C**. Advances in high-entropy alloys' microstructure, properties and preparation / C. Yang // Metals. – 2026. – V. 16. – I. 6. – P. 607-610. DOI: 10.3390/met16060607.
5. **Miracle, D.B.** High-entropy alloys: a current evaluation of founding ideas and core effects and exploring «nonlinear alloys» / D.B. Miracle // The Journal of the Minerals, Metals and Materials Society. – 2017. – V. 69. – I. 11. – P. 2130-2136. DOI: 10.1007/s11837-017-2527-z.
6. **Pickering, E.J.** High-entropy alloys: a critical assessment of their founding principles and future prospects / E.J. Pickering, N.G. Jones // International Materials Reviews. – 2016. – V. 61. – I. 3. – P. 183-202. DOI: 10.1080/09506608.2016.1180020.
7. **Wang, X.** High-entropy alloys: emerging materials for advanced functional applications / X. Wang, W. Guo, Y. Fu // Journal of Materials Chemistry A. – 2020. – V. 9. – I. 2. – P. 663-701. DOI: 10.1039/D0TA09601F.
8. **Wang, J.** High-entropy alloy coatings: a systematic review on composition design, microstructural mechanisms, and multifunctional application / J. Wang, D. Jia, Q. Gao, Y. Fu, X. Wu // Materials & Design. – 2025. – V. 258. – Art. № 114715. – 5 p. DOI: 10.1016/j.matdes.2025.114715.
9. **Mikheeva, V.I.** The hydrides of the rare-earth metals / V.I. Mikheeva, M.E. Kost // Russian Chemical Reviews – 1960 – V. 29. – I.1. – P. 28-37. DOI: 10.1070/RC1960v029n01ABEH001216.
10. **Bos, W.G.** The rare earth hydrides / W.G. Bos, K.H. Gayer // Journal of Nuclear Materials – 1966. – V. 18. – I. 1. – P. 1-30. DOI: 10.1016/0022-3115(66)90092-4.
11. **Korst, W.L.** Rare earth-hydrogen systems. I. Structural and thermodynamic properties / W.L. Korst, J.C. Warf

// Inorganic Chemistry. – 1966. – V. 5. – I. 10. – P. 1719-1726. DOI: 10.1021/ic50044a018.
12. **Jiang, Z.** Research progress of rare earth-based hydrogen storage alloys / Z. Jiang, J. Wang, D. Cao // Key Engineering Materials. – 2020. – V. 861. – P. 354-362. DOI: 10.4028/www.scientific.net/KEM.861.354.
13. **Xu, Y.** Rare-earth metal-based materials for hydrogen storage: progress, challenges, and future perspectives / Y. Xu, X. Yang, Y. Li et al. // Nanomaterials. – 2024. – V. 14. – I. 20. – P. 1671-1690. DOI: 10.3390/nano14201671.
14. **Sahlberg, M**. Superior hydrogen storage in high entropy alloys / M. Sahlberg, D. Karlsson, C. Zlotea, U. Jansson // Scientific Reports. – 2016. – V. 6. – Art. № 36770. – 6 p. DOI: 10.1038/srep36770.
15. **Karlsson, D.** Structure and hydrogenation properties of a HfNbTiVZr high-entropy alloy / D. Karlsson, G. Ek, J. Cedervall et al. // Inorganic Chemistry. – 2018. – V. 57. – I. 4. – P. 2103-2110. DOI: 10.1021/acs.inorgchem.7b03004.
16. **Zlotea, C.** Hydrogen sorption in TiZrNbHfTa high entropy alloy / C. Zlotea, M.A. Sow, G. Ek et al. // Journal of Alloys and Compounds. – 2019. – V. 775. – P. 667-674. DOI: 10.1016/j.jallcom.2018.10.108.
17. **Zhang, C.** Study on the hydrogen storage properties of a TiZrNbTa high entropy alloy / C. Zhang, A. Song, Y. Yuan et al. // International Journal of Hydrogen Energy. – 2020. – V. 45. – I. 8. – P. 5367-5374. DOI: 10.1016/j.ijhydene.2019.05.214.
18. **Li, T.** Study on the hydrogen absorption properties of a YGdTbDyHo rare-earth high-entropy alloy / T. Li, Z. Xie, W. Zhou et al. // International Journal of Minerals, Metallurgy and Materials. – 2025. – V. 32. – I. 1. – P. 127-135. DOI: 10.1007/s12613-024-2933-5.
19. **Ragg, O.M.** The HD and HDDR processes in the production of Nd-Fe-B permanent magnets / O.M. Ragg, G. Keegan, H. Nagel, I.R. Harris // International Journal of Hydrogen Energy. – 1997. – V. 22. – I. 2-3. – P. 333-342. DOI: 10.1016/S0360-3199(96)00174-7.
20. **Poenaru, I.** HDDR as advanced processing method and recycling technology to address the rare-earth resource criticality in high performance $Nd_2Fe_{14}B$ magnets production / I. Poenaru, E.A. Patroi, D. Patroi, A. Iorga, E. Manta // Journal of Magnetism and Magnetic Materials. – 2023. – V. 577. – Art. № 170777. – 19 p. DOI: 10.1016/j.jmmm.2023.170777.
21. **Liu, R.** Features of the solid HDDR process in sintered (Nd,Pr,Gd)-Fe-B magnets at low hydrogen pressure and low temperature / R. Liu, I.I. Bulyk, M. Yang, Y. Wang, H. Wang // Materials. – 2025. – V. 18. – I. 17. – P. 4019-4036. DOI: 10.3390/ma18174019.
22. **Huot, J.** Mechanochemistry of metal hydrides: recent advances / J. Huot, F. Cuevas, S. Deledda et al. // Materials. – 2019. – V. 12. – I. 17. – Art. № 2778. – 44 p. DOI: 10.3390/ma12172778.
23. **Duwal, S.** Enhancement of hydrogen absorption and hypervalent metal hydride formation in lanthanum using cryogenic ball milling / S. Duwal, V. Stavila, C. Spataru et al. // arXiv:2506.23980. – 2025. – 24 p. DOI: 10.48550/arXiv.2506.23980.
24. **Pommerin, A.** Influence of the ball milling conditions on the preparation of rare earth aluminum hydrides / A. Pommerin, M. Felderhoff, F. Schüth, C. Weidenthaler // Scripta Materialia. – 2010. – V. 63. – I. 11. – P. 1128-1131. DOI: 10.1016/j.scriptamat.2010.08.020.
25. **Zaluski, L.** Nanocrystalline metal hydrides / L. Zaluski., A. Zaluska, J.O. Ström-Olsen // Journal of Alloys and Compounds. – 1997. – V. 253-254. – P. 70-79. DOI: 10.1016/S0925-8388(96)02985-4.
26. **Nielsen, T.K.** Nanoconfined hydrides for energy storage / T.K. Nielsen, F. Besenbacher, T.R. Jensen // Nanoscale. – 2011. – V. 3. – I. 5. – P. 2086-2098. DOI: 10.1039/c0nr00725k.
27. **Palmero, P**. Structural ceramic nanocomposites: a review of properties and powders' synthesis methods / P. Palmero // Nanomaterials. 2015. – V. 5. – I. 2. – P. 656-696. DOI: 10.3390/nano5020656.
28. **Luo, Y.** Enhanced hydrogen storage/sensing of metal hydrides by nano-modification / Y. Luo, Q. Wang, J. Li et al. // Materials Today Nano. – 2019. – V. 9. – Art. № 100071. – 87 p. DOI: 10.1016/j.mtnano.2019.100071.
29. **Preiur, D.** Size dependence of lattice parameter and electronic structure in CeO_2 nanoparticles / D. Preiur, W. Bonani, K. Popa et al. // Inorganic Chemistry. – 2020. – V. 59. – I. 8. – P. 5760-5767. DOI: 10.1021/acs.inorgchem.0c00506
30. **Jagiello, K.** Size-dependent electronic properties of nanomaterials: how this novel class of nanodescriptors supposed to be calculated? / K. Jagiello, B. Chomicz, A. Avromopoulos et al. // Structural Chemistry. – 2017. – V. 28. – I. 3. – P. 635-643. DOI: 10.1007/s11224-016-0838-2
31. **Caizer, C.** Nanoparticle size effect on some magnetic properties / C. Cazier // In: Handbook of Nanoparticles. – Amsterdam: Springer, 2015. – P. 475-519. DOI: 10.1007/978-3-319-15338-4_24.
32. **Issa, B.** Magnetic nanoparticles: surface effects and properties related to biomedicine applications / B. Issa, I.M. Obaidat, B.A. Albiss, H. Yousef // International Journal of Molecular Sciences. – 2013. – V. 14. – I. 11. – P. 21266-21305. DOI: 10.3390/ijms141121266.
33. **Vajda, P.** Commensurate and incommensurate magnetic structures in rare-earth hydrides / P. Vajda, G. Andre // Journal of Alloys and Compounds. – 2001. – V. 326. – I. 1-2. – P. 151-156. DOI: 10.1016/S0925-

8388(01)01251-8.
34. **Piquer, C.** A phenomenological model for the rare-earth contribution to the magnetic anisotropy in $RFe_{11}Ti$ and $RFe_{11}TiH$ / C. Piquer, F. Grandjean, O. Isnard, G.J. Long // Journal of Physics: Condensed Matter. – 2006. – V. 18. – № 1. – P. 221-242. DOI: 10.1088/0953-8984/18/1/016.
35. **Skomski, R.** RKKY interactions between nanomagnets of arbitrary shape / R. Skomski // EDP Sciences Europhysics Letters. – 1999. – V. 48. – I. 4. – P. 455-460. DOI: 10.1209/epl/i1999-00504-y.
36. **Mi, S.** Size effect of Ruderman–Kittel–Kasuya–Yosida interaction mediated by electrons in nanoribbons / S. Mi, S.-H. Yuan, P. Lyu // Journal of Applied Physics. – 2011. – V. 109. – I. 8. – Art. №. 083931. – 4 p. DOI: 10.1063/1.3575338.
37. **Lundin, C.E.** Research on the samarium-type intermediate phases of intra-rare-earth binary systems – AD-633558 (also Given as DRI-2326, Final Report) / C.E. Lundin. – Denver: Denver Research Institute, University of Denver, CO, USA, 1966. – 32 p.
38. **Jayaraman, A.** Pressure-induced phase transformations and magnetic ordering in some intra-rare-earth alloys and samarium / A. Jayaraman, R.C. Sherwood, H.J. Williams, E. Corenzwit // Physical Review. – 1966. – V. 148. – I. 2. – P. 502-508. DOI: https://doi.org/10.1103/PhysRev.148.502.
39. **Ellner, M.** The structure of the trihydride GdH_3 / M. Ellner, H. Reule, E.J. Mittemeijet // Journal of Alloys and Compounds. – 2000. – V. 309. – I. 1-2. – P. 127-131. DOI: https://doi.org/10.1016/S0925-8388(00)01055-0.
40. **Mannsman, M.** The structure of HoD_3 / M. Mansmann, W.E. Wallace // Journal de Physique. – 1964. – V. 25. – I. 5. – P. 454-459. DOI: 10.1051/jphys:01964002505045400.
41. **Uporov, S.A.** Magnetocaloric effect in ScGdTbDyHo high-entropy alloy: Impact of synthesis route / S.A. Uporov, S.Kh. Estemirova, E.V. Sterkhov et al. // Intermetallics. – 2022. – V 151. – Art. №. 107678. – 10 p. DOI: 10.1016/j.intermet.2022.107678.
42. **Qiao, J.W.** Rare-earth high entropy alloys with hexagonal close-packed structure / J.W. Qiao, M.L. Bao, Y.J. Zhao et al. // Journal of Applied Physics. – 2018. – V. 124. – I. 19. – Art. №. 195101. – 7 p. DOI: 10.1063/1.5051514.
43. **Soler, R.** Microstructural and mechanical characterization of an equiatomic YGdTbDyHo high entropy alloy with hexagonal close-packed structure / R. Soler, A. Evirgen, M. Yao et al. // Acta Materialia. – 2018. – V. 156. – P. 86-96. DOI: 10.1016/j.actamat.2018.06.010.
44. **Jordan, R.B**. The lanthanide contraction: what is abnormal and why? / R.B. Jordan // Inorganic Chemistry 2025. – V. 64. – I. 5. – P. 2207-2216. DOI: 10.1021/acs.inorgchem.4c03698.
45. **Mugiraneza, S.** Tutorial: a beginner's guide to interpreting magnetic susceptibility data with the Curie-Weiss law / S. Mugiraneza, A.M. Hallas // Communications Physics. – 2022. – V. 5. – Art. №. 95. – 12 p. DOI: 10.1038/s42005-022-00853-y.
46. **Wang, L.** Multi-principal rare-earth Gd-Tb-Dy-Ho-Er alloys with high magnetocaloric performance near room temperature / L. Wang, Z. Lu, H. Guo et al. // Journal of Alloys and Compounds. – 2023. – V. 960. – Art. № 170901. – 10 p. DOI: 10.1016/j.jallcom.2023.170901.
47. **Кудреватых, Н.В.** Магнетизм редкоземельных металлов и их интерметаллических соединений / Н.В. Кудреватых, А.С. Волегов. – Екатеринбург: Изд-во Уральского университета, 2015. – 198 с.
48. **Yuan, Y.** Rare-earth high-entropy alloys with giant magnetocaloric effect / Y. Yuan, Y. Wu, X. Tong et al. // Acta Materialia. – 2017. – V. 125. – P. 481-489. DOI: 10.1016/j.actamat.2016.12.021.
49. **Lu, S.F.** Magnetocaloric effect of high-entropy rare-earth alloy GdTbHoErY / S.F. Lu, L. Ma, G.H. Rao et al. // Journal of Materials Science: Materials in Electronics. – 2021. – V. 32. – I. 8. – P. 10919-10926. DOI: 10.1007/s10854-021-05749-1.
50. **Svalov, A.V.** Magnetocaloric effect in powder of GdTbDyHoEr high-entropy alloy / A.V. Svalov, D.S. Neznakhin, A.V. Arkhipov et al. // Physics of the Solid State. – 2024. – V. 66. – I. 12. – P. 2120-2124. DOI: 10.61011/PSS.2024.12.60204.313.
51. **Никитин, С.А.** Магнитные свойства редкоземельных металлов и их сплавов / С.А. Никитин. – М.: Издательство МГУ, 1989. – 248 с.
52. **Pankratov, N.Yu.** Structure and magnetic properties of the medium-entropy GdTbDyY alloy / N.Yu. Pankratov, I.S. Tereshina, P.A. Krot, V.N. Verbetsky, S.A. Nikitin // Bulletin of the Russian Academy of Sciences: Physics. – 2025. – V. 89. – I. 4. – P. 572-577. DOI: 10.1134/S1062873825710785.
53. **Flood, D.J.** Crystal fields and magnetic properties of ErH_3 / D.J. Flood // Journal of Applied Physics. – 1978. –V. 49. – I. 2. – P. 1495-1497. DOI: 10.1063/1.324933.
54. **Carlin, R.L.** Magnetic ordering in GdH_3 / R.L. Carlin, R.D. Chirico, K.O. Joung et al. // Physics Letters A. – 1980. – V. 75. – I. 5. – P. 413-414. DOI: 10.1016/0375-9601(80)90858-0.
55. **Carlin, R.L**. Magnetic ordering in DyH_2 and DyH_3 / R.L. Carlin, L.J. Krause // Chemical Physics Letters. – 1981. – V. 82. – I. 2. – P. 323-326. DOI: 10.1016/0009-2614(81)85165-2.